Modeling polymorphic ventricular tachycardia at rest using patient-specific induced pluripotent stem cell-derived cardiomyocytes

Yvonne Sleiman, Monia Souidi, Ritu Kumar, Ellen Yang, Fabrice Jaffré, Ting Zhou, Albin Bernardin, Steve Reiken, Olivier Cazorla, Andrey Kajava, et al.

▶ **To cite this version:**

Yvonne Sleiman, Monia Souidi, Ritu Kumar, Ellen Yang, Fabrice Jaffré, et al.. Modeling polymorphic ventricular tachycardia at rest using patient-specific induced pluripotent stem cell-derived cardiomyocytes. EBioMedicine, 2020, 60, pp.103024. 10.1016/j.ebiom.2020.103024 . hal-03089303v1

HAL Id: hal-03089303

https://hal.science/hal-03089303v1

Submitted on 4 Nov 2020 (v1), last revised 3 Jun 2021 (v2)

HAL is a multi-disciplinary open access archive for the deposit and dissemination of scientific research documents, whether they are published or not. The documents may come from teaching and research institutions in France or abroad, or from public or private research centers.

L'archive ouverte pluridisciplinaire **HAL**, est destinée au dépôt et à la diffusion de documents scientifiques de niveau recherche, publiés ou non, émanant des établissements d'enseignement et de recherche français ou étrangers, des laboratoires publics ou privés.

Modeling polymorphic ventricular tachycardia at rest using patient-specific induced pluripotent stem cell-derived cardiomyocytes

Yvonne Sleiman[a], Monia Souidi[a], Ritu Kumar[b], Ellen Yang[b], Fabrice Jaffré[b], Ting Zhou[b], Albin Bernardin[a], Steve Reiken[c], Olivier Cazorla[a], Andrey V. Kajava[d], Adrien Moreau[1], Jean-Luc Pasquié[a,e], Andrew R. Marks[c], Bruce B. Lerman[f], Shuibing Chen[b], Jim W. Cheung[f], Todd Evans[b], Alain Lacampagne[a], Albano C. Meli[a,*]

[a] *PhyMedExp, Inserm, CNRS, University of Montpellier, Montpellier, France*
[b] *Department of Surgery, Weill Cornell Medical College, New York, NY, United States*
[c] *Department of Physiology and Cellular Biophysics, Clyde and Helen Wu Center for Molecular Cardiology, Columbia University College of Physicians and Surgeons, New York, NY, United States*
[d] *CRBM, CNRS, University of Montpellier, Montpellier, France*
[e] *Department of Cardiology, CHU of Montpellier, Montpellier, France*
[f] *Division of Cardiology, Weill Cornell Medical College, New York, NY, United States*

Keywords:
PMVT
Ryanodine receptor
hiPSC-derived cardiomyocytes
Calcium handling
Contractile properties

A B S T R A C T

Background: While mutations in the cardiac type 2 ryanodine receptor (RyR2) have been linked to exercise-induced or catecholaminergic polymorphic ventricular tachycardia (CPVT), its association with polymorphic ventricular tachycardia (PMVT) occurring at rest is unclear. We aimed at constructing a patient-specific human-induced pluripotent stem cell (hiPSC) model of PMVT occurring at rest linked to a single point mutation in RyR2.

Methods: Blood samples were obtained from a patient with PMVT at rest due to a heterozygous RyR2-H29D mutation. Patient-specific hiPSCs were generated from the blood samples, and the hiPSC-derived cardiomyocytes (CMs) were generated via directed differentiation. Using CRIPSR/Cas9 technology, isogenic controls were generated by correcting the RyR2-H29D mutation. Using patch-clamp, fluorescent confocal microscopy and video-image-based analysis, the molecular and functional properties of RyR2-H29D hiPSC—CMs and control hiPSC—CMs were compared.

Findings: RyR2-H29D hiPSC—CMs exhibit intracellular sarcoplasmic reticulum (SR) Ca^{2+} leak through RyR2 under physiological pacing. RyR2-H29D enhances the contribution of inositol 1,4,5-trisphosphate receptors to excitation-contraction coupling (ECC) that exacerbates abnormal Ca^{2+} release in RyR2-H29D hiPSC—CMs. RyR2-H29D hiPSC—CMs exhibit shorter action potentials, delayed afterdepolarizations, arrhythmias and aberrant contractile properties compared to isogenic controls. The RyR2-H29D mutation causes post-translational remodeling that is fully reversed with isogenic controls.

Interpretation: To conclude, in a model based on a RyR2 point mutation that is associated with short-coupled PMVT at rest, RyR2-H29D hiPSC—CMs exhibited aberrant intracellular Ca^{2+} homeostasis, shortened action potentials, arrhythmias and abnormal contractile properties.

Funding: French Muscular Dystrophy Association (AFM; project 16,073, MNM2 2012 and 20,225), "Fondation de la Recherche Médicale" (FRM; SPF20130526710), "Institut National pour la Santé et la Recherche Médicale" (INSERM), National Institutes of Health (ARM; R01 HL145473) and New York State Department of Health (NYSTEM C029156).

Introduction

Single-point mutations in cardiac ryanodine receptor/calcium (Ca^{2+}) release channel (RyR2) are associated with catecholaminergic PMVT (CPVT) under stress conditions [1-3]. However, mutations in

One Sentence Summary: RyR2 calcium leak causing PMVT at rest

* To whom correspondence should be addressed: Albano C. Meli, Ph.D., PhyMedExp, INSERM U1046, CNRS UMR9214, University of Montpellier, CHU Arnaud de Villeneuve, 371 Avenue du Doyen G. Giraud, 34295, Montpellier cedex 5, France.
E-mail address: albano.meli@inserm.fr (A.C. Meli).

Evidence before this study

Previously, we showed that the recombinant RyR2-H29D mutant expressed in a heterologous system causes a gain-of-function with increased open probability, opening frequency and sensitivity to low diastolic calcium at rest.

Added value of this study

Using patient-specific hiPSC—CMs, we found that this single-point mutation RyR2-H29D is associated with several key properties including aberrant SR Ca^{2+} leak under physiological pacing, pro-arrhythmic electrical phenotypes, impaired and asynchronous contractile properties and aberrant RyR2 post-translational modifications, all under non-stress conditions. Our study adds to the growing body of evidence that RyR2 mutations can be associated with inherited forms of arrhythmias occurring at rest and not during exertion or exercise. Our hiPSC—CM model of short coupled PMVT provides insights into abnormal RyR2 behavior that may help guide mechanism-specific therapy.

Implications of all the available evidence

Although early descriptions of the entity of short-coupled Torsades de pointe identified verapamil as the therapy of choice for arrhythmia suppression, it is possible that treatment of RyR2 variant-associated PMVT with RyR2-targeted therapy such as flecainide and Rycal compounds would be beneficial. Further study on the electrophysiological response of RyR2-H29D hiPSC—CMs to different pharmacological therapies would help shed further light on the clinical implications of our findings.

RyR2 have also been linked with arrhythmias at rest [4] and to short-coupled PMVT [5]. We previously reported a novel RyR2-H29D mutation harbored by a mother and her daughter associated with a clinical phenotype of short-coupled PMVT at rest [4]. In contrast to CPVT patients, these 2 patients experienced short-coupled PMVT and syncope at rest and not during exertion. By expressing recombinant RyR2 in a heterologous system, we showed that the RyR2-H29D mutation, in contrast to CPVT RyR2 mutations, causes a leaky RyR2 channel at diastolic Ca^{2+} levels under non-stress conditions with a slight depletion of the RyR2-stabilizing protein calstabin2 from the RyR2 macromolecular complex. We proposed a model for the pathophysiology behind RyR2-H29D in which increased sarcoplasmic reticulum (SR) Ca^{2+} leak at rest activates the sodium/calcium exchanger (NCX) and produces delayed afterdepolarizations (DADs) leading to short-coupled premature ventricular contractions (PVCs) and PMVT [4].

However, recombinant protein expression in heterologous systems and animal models do not always recapitulate human cardiac pathophysiology [6]. For example, the mouse resting heart rate is approximately ten-fold faster than that of humans and mouse cardiomyocytes (CMs) have different electrical properties compared to human CMs. Therefore, it is essential to develop human cardiac models to better characterize the consequences of such mutations in human pathophysiology. Human induced pluripotent stem cells (hiPSCs) offer great opportunities for disease modeling, drug screening and regenerative medicine [7]. To investigate the molecular mechanisms underlying short coupled PMVT at rest associated with RyR2 single point mutations, we collected a blood sample from an affected patient harbouring the RyR2-H29D mutation to generate mutant iPSC lines, which were subsequently differentiated into hiPSC-derived cardiomyocytes (hiPSC—CMs). To compare the cellular and molecular impacts of the RyR2-H29D mutation in the patient-specific genetic background, we generated an isogenic control line by correcting the RyR2-H29D mutation using CRIPSR/Cas9 technology.

Materials and methods

Ethics statement

Written informed consent was obtained from the patient carrying the RyR2-H29D mutation who agreed to have blood samples obtained for hiPSC generation. This study was conducted in accordance with the Declaration of Helsinki and approved by the Cornell Institutional Review Board Committee of Weill Cornell Medicine (NY, USA).

Cell lines

To generate hiPSCs, peripheral blood mononuclear cells (PBMCs) were first isolated from 5cc whole blood by Ficoll density gradient centrifugation. From this, erythroblasts were expanded for 12 days in expansion medium [EM: QBSF-60 hematopoietic stem cell media (Quality Biologicals) supplemented with 50 ng/ml SCF, 10 ng/ml IL3, 2 U/ml EPO, 40 ng/ml IGF1, 1 μM dexamethasone (Sigma), 100 μg/ml Primosin (Invitrogen) and 50 μg/ml L-Ascorbic acid (Sigma). 1×105 erythroblasts (CD71-positive) were transduced for 12 hr with Sendai viral vectors (CytoTuneTM, Life Tech,) expressing human OCT3/4, SOX2, KLF4, cMYC. Following transduction cells were cultured for an additional 2 days in EM. Cells were then plated on mouse embryo fibroblasts (MEFs, GlobalStem, ThermoFisher) and cultured for two days in iPSC medium [DMEM/F12 (Life Tech.), 10% FBS (Sigma), 1% MEM-NEAA (Life Tech.), 2 mM L-Glutamine (Life Tech.), 1% Pen/Strep (Life Tech.), 0.1 mM 2-mercaptoethanol (Life Tech.), 10 ng/ml bFGF and 50 ug/ml L-Ascorbic acid (Sigma)], supplemented with EM growth factors, then for two days in hiPSC medium without growth factors, and then for one day in hiPSC:hESC (1:1) medium. The composition of hESC medium was similar to hiPSC medium except that 10% FBS was replaced by 20% KOSR (Life Tech). Thereafter cells were reprogrammed in the hESC medium, which was changed every day. Multiple iPSC colonies were picked approximately 3 weeks after transduction and expanded on MEFs in hESC medium for 10 passages. All cytokines were purchased from R&D systems. Several hiPSC clones were treated with 50 μL/mL Colcemid (Invitrogen), and submitted to the Molecular Cytogenetics Core at Memorial Sloan Kettering Cancer Center for karyotyping, and only those with normal karyotype were studied further. 2 independent clones of PMVT RyR2-H29D hiPSC (C1, C3) were used in this study in addition to an isogenic control hiPSC (PMVT-29-corrected, described below) and a commercial healthy control gender-matched line, UB47, previously described [8]. Cells were maintained either as colonies or single cells on Matrigel hES-qualified (Corning, 354,277) as previously described [8]. Briefly, the colonies were manually dissected using a needle and passaged every 4–6 days whereas the single cells were enzymatically dissociated using Tryple enzyme (Gibco, ref: 12,604–013) and passaged every 4 days.

CRISPR/Cas9 correction

The patient hiPSCs carried a heterozygous point mutation (*C>G* mutation) on exon 2 of the RYR2 gene. A targeting CRISPR sgRNA was designed using the web resource at https://www.benchling.com/crispr/. The target sequence was cloned into the pX330-U6-Chimeric_BB-CBh-hSpCas9 vector (Addgene plasmid #42,230). The template ssODN was designed to contain the correct nucleotide and a silent mutation on the "PAM" of the sgRNA target, so that the donor would not be recut by Cas9. The ssODN was purchased from IDT. The

sgRNA-target and ssODN sequence are listed in Table S1. To perform the gene correction, patient-derived hiPSCs were expanded in the absence of MEFs in TeSRTM-E8TM media (Stem Cell Technologies), dissociated using Accutase (STEM CELL) and electroporated (1×106 cells per reaction) with 4 μg sgRNA-construct plasmid and 4 ul ssODN (10 μM stock) using Human Stem Cell NucleofectorTM solution (Lonza) following manufacturer's instructions. The cells were then seeded, and 4 days later, dissociated into single cells with Accutase (STEM CELL) and re-plated at a low density (4 per well in 96-well plates) to obtain the single-cell clones. 10 days later, individual colonies were passaged to generate two copies of each, one of which was analysed by PCR and DNA sequencing, and the other used to expand. The PCR and sequencing primers are listed in Table S1. The sequencing results showed the gene corrected hiPSC clone (clone #22) has converted the mutation (G to C) and carried a silent mutation on the "PAM" (Fig. S1C).

The top ranked sgRNA for targeting the *RYR2* gene within 100 bp on either side of the variant was designed using the CHOPCHOP software program [9]. The specificity of this sgRNA was subsequently analysed using the software program Benchling (Benchling.com), which uses methodology previously described [10]. Scores above 50 are considered to be good guides, and the score of this sgRNA was 55.8. All potential off-target sites are listed in Table S2. Only one off-target site is located in a gene, SCUBE1, with a calculated efficiency 0.7% compared to the 100% on-target site.

Karyotype

DAPI-banded karyotyping was performed by the Molecular Cytogenetics Core Facility, Memorial Sloan Kettering Cancer centre, New York.

Molecular modeling of the ryr2-h29d mutant

To further understand how the H29D substitution may change the structure of human RyR2, we modelled this mutant based on the known structure of the pig RyR2 (PDB code 5GO9) as previously described [8].

Cardiac differentiation

A 2D sandwich-based protocol was used to differentiate the hiPSC lines to the cardiac lineage as previously published [8]. Briefly, undifferentiated hiPSC colonies were plated into 6 well dishes in standard conditions (21% O_2 and 5% CO_2 at 37° C). At 90% confluency (day-1), 0.04 mg of Matrigel reduced growth factor (MgFr) was added in Stemflex medium (Gibco, A33493–01). On day 0, mesoderm was induced by adding 6 μM CHIR99021 (Calbiochem, ref: 3,615,715) and 0.04 mg of Matrigel growth factor reduced (MgFr) (Corning, ref: 356,231) in RPMI 1640-B27-minus insulin medium (Gibco, ref: 21,875–034). On day 2, the medium was changed with RPMI 1640-B27-minus insulin. On day 3, cardiac progenitor formation was induced by adding 2 μM Wnt inhibitor C59 (Wnt C59) (Tocris, ref: 5148/10) in RPMI 1640-B27-minus insulin; the medium was kept 2 days. On day 5, the medium was changed to RPMI 1640-B27-minus insulin and was kept until day 9 and then renewed every 2 days. On day 9, the medium was changed to RPMI 1640-B27 and was kept until day 50; the medium was renewed every 2 days. On day 20, the hiPSC—CMs were purified using a glucose-, and pyruvate-free and lactate-based medium as previously described [11]. On day 50, the cells were treated 10 days with the commercially-available Pluricyte medium (Ncardia, ref: PM-2100) which was renewed every 3 days.

Flow cytometry

At day 15 of differentiation, cells were individualized using trypsin-EDTA for 5 min at 37 °C. Flow cytometry was performed as previously described [12] using mouse anti-cTNT antibody (ThermoScientific, #MA5–12,960).

qRT-PCR

30-day-old beating monolayer cells were used for RNA extraction. Total RNA was isolated using a NucleoSpin RNA kit (Macherey-Nagel, ref: 740,955.50) followed by reverse transcription to obtain cDNA using the Transcriptor Universal cDNA Master kit (Roche, ref: 05,893,151,001), according to manufacturers' protocols. For detection of cardiac markers cDNA was amplified by LightCycler 480 SYBR Green I Master (Roche, ref: 04,707,516,001) for qRT-PCR. Glyceraldehyde-3-Phosphate Dehydrogenase (*GAPDH*) was used as a reference gene. Primers for relative human cardiac marker expression are listed in a previously published study [8] except the DHPR primers: H1_CACNA1C (Forward: GGAGAGTTTTCCAAAGAGAG, Reverse: TTTGAGATCCTCTTCTAGCTG) and H1_CACNA1D (Forward: AAAATGGGCATCATTCTTCC, Reverse: AGTTTCATAATAGCGGGTTC).

Monolayer dissociation of hiPSC—CMs

48-day-old beating (contracting) monolayer regions were dissociated in order to isolate CMs by washing the monolayer cells twice with Ca^{2+}- and Mg^{2+}-free PBS (Sigma, ref: D8537). The cells were detached by incubating them for 10 min at 37 °C with pre-warmed TrypLE (Gibco) with periodic shaking. RPMI 1640-B27 was added to stop the activity of TrypLE. Cell clumps were then filtered using a 37 μm reversible strainer (Stemcell Technologies, ref: 27,215). A centrifugation for 5 min at 200 g obtained a cell pellet that was resuspended with RPMI 1640-B27 containing ROCK inhibitor. The cells (10 000 cells/Cm^2) were plated on dishes pre-coated with Matrigel hES-qualified in RPMI 1640-B27 medium.

Immunocytochemistry

To validate hiPSC pluripotency, immunostaining was performed by fixing cells in culture dishes with 4% paraformaldehyde (PFA, Sigma) at RT for 20 min. Blocking was performed for an hour by incubating cells in PBS supplemented with 10% FBS, 0.1% IgG-free BSA (Jackson ImmunoResearch) and 0.1% saponin from quillaja bark (Sigma) at RT. Cells were incubated overnight at 4 °C with anti-NANOG (Abcam), anti-OCT-4 (Santa Cruz), anti-SSEA-4 (Millipore) and anti-TRA-1–81 (Invitrogen) in blocking buffer. Fluorescence-conjugated secondary antibody was used for visualization. Images were collected on a Zeiss epifluorescence microscope with AxioVision software.

For detection of sarcomeric cardiac markers, namely α-actinin, cTnI and cTnT, dissociated beating monolayer cells were fixed with 4% PFA, 4% sucrose for 20 min at 37 °C and washed 3 times in PBS for 3 min each. They were then permeabilized and blocked with PBS containing 1% bovine serum albumin (BSA) and 0.1% triton for 30 min at room temperature and washed 3 times with PBS for 3 min each. Primary antibodies (anti-α-actinin from Sigma, ref: A7811, anti-TnI from Hytest, ref: 4T21 and anti-TnT from ThermoFisher Scientific, ref: MS-95-P1) were incubated at 4 °C overnight diluted at 1:200 in 1% PBS, 1% BSA. The next day, Alexa 555 secondary antibodies (Life Tech, ref: A31570) were applied at 1:250. DAPI at 0.1 μg/ml was applied for 1 h at RT. Samples were washed 3 times with PBS for 10 min and mounted in antifade liquid medium (Thermo Fisher, ref: P36930). Images were collected on an inverted confocal fluorescent microscope equipped with Zeiss LSM780 confocal and 63x lens (oil immersion, numerical aperture, N.A. = 1.4) with Zen software.

Immunoprecipitation and immunoblot analyses

Differentiated cardiomyocytes of at least 30-day-old were incubated with a lysis buffer composed of 35 mM NaF, 50 mM Tris maleate pH 6.8, 1 mM Na_3VO_4 and protease inhibitors. RyR2 channels were immunoprecipitated by incubating 100 μg of cell lysate using an anti-RyR antibody (homemade antibody: rabbit 5029 y2) for 2 h at 4 °C in 0.5 ml of a RIPA buffer (10 mM Tris−HCl pH 7.4, 150 mM NaCl, 5 mM NaF, 1 mM Na_3VO_4, 1% Triton-X100, and protease inhibitors). The immune samples were then incubated with protein A sepharose beads (GE Healthcare, ref: 17−5280−01) overnight at 4 °C, after which the beads were washed three times with RIPA buffer. Proteins were then separated using a 4−20% SDS-PAGE gradient gel, blotted onto nitrocellulose membranes, and incubated overnight at 4 °C with primary antibodies: rabbit 5029 Y2 anti-RyR2 (1:5000), anti-phospho-RyR2-pSer2809 (homemade antibody: polyclonal rabbit CRTRRI-(pS)-QTSQ, 1:1000), anti-RyR2-pSer2815 (homemade antibody: polyclonal rabbit CSQTSQV-(pS)-VD), anti-Cys-NO (Sigma-Aldrich, 1:1000), anti-DNP antibody (Millipore,1:2000), tubulin (Abcam, ref: EPR13796) and mouse anti-FKBP12.6 (Santa Cruz, ref: 376,135, 1:1000). Levels of RyR2 bound proteins were normalized to the total RyR2 immunoprecipitated (arbitrary units). All immunoblots were developed using the Odyssey system (LI-COR) with IR labeled secondary antibodies (1:30,000 dilution) for 1 h at room temperature.

Measurement of cytosolic Ca^{2+} variation under fluorescent confocal microscopy

60-day-old contracting monolayer cells were enzymatically dissociated into cardiomyocytes to measure and analyze the intracellular Ca^{2+} variations in hiPSC-derived cardiomyocytes. To monitor the intracellular Ca^{2+} spatial dynamics, hiPSC—CMs were loaded with 1.5 μM of non-ratiometric but highly sensitive Fluo-4 AM Ca^{2+}indicator (Molecular Probes) for 15 min. Ca^{2+} images were recorded in line-scan mode with an inverted confocal fluorescent microscope equipped with Zeiss LSM780 confocal and 63x lens (oil immersion, numerical aperture, N.A. = 1.4) and Fluo-4 AM was excited at 488 nm. Confocal images were obtained in line scan mode (i.e. x-t mode, 1.53 ms per line; 512 pixels x 5000 lines) using Zen (Zeiss). The maximal amplitude, frequency of events, Ca^{2+} release velocity of the raising phase and the decay phase time were analyzed using the Peak-inspector algorithm made via Python 3 (https://www.python.org/download/releases/3.0/) as previously done [8]. The tetracaine/caffeine experiments were used to measure the SR Ca^{2+} leak/load in a 0 Na^+, 0 Ca^{2+}Tyrode solution (140 mM LiCl, 5.4 mM KCl, 0.53 mM MgCl2, 5 mM HEPES, 10 mM glucose, 10 mM EGTA, pH 7.4 with LiOH). Following the 1 Hz pacing, the hiPSC—CMs were superfused with Na^+- and Ca^{2+}-free solutions, prior to the addition of 1 mM tetracaine. Tetracaine was applied for 60 s and washed-out with the Na^+- and Ca^{2+}-free solution prior to the addition of 30 mM caffeine. The acquisition was performed in plane (frame) scan mode in x-y mode at a rate of 1 image/0.782 s. To enable comparisons between cells, changes in the Fluo-4 fluorescence signal (ΔF) were normalized by basal fluorescence (F_0). The reduction amplitude in baseline due to tetracaine was expressed as a percentage of the caffeine response for leak comparisons between samples. All experiments were performed at room temperature. All data were extracted using Zen (Zeiss).

Diastolic calcium levels at rest and under stress were assessed using the ratiometric fluorescent Ca^{2+} indicator Indo1-AM (Invitrogen). The Indo1-loaded hiPSC—CMs (2 μM for 15 min at 37 °C) were excited at 360 nm, and the resulting whole cell fluorescence was measured simultaneously at 405 and 480 nm (Ionoptix system) on a Zeiss microscope (40X oil objective). The intracellular Ca^{2+} level was measured after background subtraction using IonWizard data acquisition software.

Patch-clamp experiments

Patch-clamp experiments were performed using an Axopatch 200B amplifier (Axon Instruments) at room temperature at least 10 days after the dissociation of the hiPSC—CMs in maturation medium. The pipettes were made from borosilicate glass capillaries and were fire polished. Action potentials (APs) were evaluated using the whole-cell configuration of the patch clamp technique (in current clamp mode with a sampling frequency of 5000 Hz). Spontaneous APs were recorded using the gap free mode during which electrical activity is recorded without intervention. After artificially lowering the maximum diastolic potential to −80 mV, APs were also elicited using a 3 ms, 200 to 2500-pA rectangular current pulse injection at several frequencies. The patch pipets (resistance 2−8 mΩ) were filled with a solution containing (in mM): 10 NaCl, 122 KCl, 1 MgCl2, 1 EGTA, and 10 Hepes. The pH was adjusted to 7.3 with KOH. The external current clamp solution was composed of (in mM): 154 NaCl, 5.6 KCl, 2 CaCl2, 1 MgCl2, 8 D-glucose, and 10 Hepes. The pH was adjusted to 7.3 with NaOH. All experiments were performed at room temperature. Data were analyzed using custom written MatLab (The MathWorks Inc.), Microsoft Excel 2016 and GraphPad Prism (version 7).

Measurement of contractile properties by video-edge capture

For measurement of contractile properties, 6 well plates containing the hiPSC-derived CMs (without any cellular dispersion) were incubated in a thermostatic chamber at 21% O_2 and 5%CO_2 at 37 °C (humid atmosphere) under an inverted microscope Zeiss observer 7 equipped with a 20x objective (N.A. = 0.4). Cells were allowed to stabilize for at least 15 min prior to any recordings. Images were recorded with an Orca Falsh4 camera (Hamamatsu) with an imaging frequency of 33 ms, at 16-bit depth and a duration of 25 s per position. Using Zen, different positions of videos were chosen based on the contracting cardiac areas. The hiPSC—CM monolayer spontaneous contractile function was evaluated using a patented custom-made video analysis software (MATLAB). Phase contrast videos were acquired at 30 frames per second. After TIFF extraction, videos were processed. Contrasted particle displacement was tracked frame by frame for each video. The displacement of each contrasted particle was then processed through time resulting in a curve of the displacement as a function of time. Areas with similar contractile behavior were clustered and contractile parameters were quantified. All movies displayed in this study are at 30 frames per second.

Statistical analysis

Normality was tested using the Shapiro-Wilk test. An unpaired *t*-test was used to compare 2 independent groups with parametric distribution. A Mann-Whitney test was performed for comparing 2 independent groups non-parametric distribution. All data are expressed as mean±SEM. A value of $p < 0.05$ was considered significant. *, $p < 0.05$, **, $p < 0.01$ otherwise specified. Data analysis and statistics were done with GraphPad Prism (version 7).

Results

Generation of hiPSC carrying the RyR2-H29D variant allele and isogenic control hiPSCs with corrected variant

Using blood samples from a study patient carrying the RyR2-H29D allele, erythroblasts were expanded in culture, and reprogrammed by transduction with Sendai virus vectors expressing OCT3/4, SOX2, KLF4, and cMYC. Individual clones were isolated and expanded. Two independent clones were verified to harbor the variant allele by DNA-sequencing and to be pluripotent stem cells based

on expression of OCT4, NANOG, SSEA-4, and TRA-1−81 (Supplemental Fig. S1b). The clones were also confirmed to have a normal chromosomal content by karyotyping (Supplemental Fig. S1a). One of the clones was then used to create an isogenic control line. Following transduction with vectors expressing Cas9 and a targeting sgRNA, along with a single-stranded oligomer donor, individual clones were isolated and evaluated by DNA sequencing, which identified one clone that converted the mutation (G to C) and carried a silent mutation at the "PAM" site (Supplemental Fig. S1c). This isogenic control line was also validated as normal by karyotype (Supplemental Fig. S1a).

The RyR-H29D variant does not impact the efficiency of cardiac differentiation

To determine whether the RyR-H29D mutation affects cardiac differentiation, we used a directed differentiation protocol to generate cardiomyocytes from the patient-derived hiPSCs and the corrected isogenic control. Flow cytometry was used to analyze efficiency of differentiation based on cardiac troponin T (cTnT) expression at day 15. We found no significant differences in the efficiency for generation cTnT-postive cardiomyocytes in the RyR2-H29D cells (58.33± 9.82%) compared to the isogenic control hiPSC—CMs (64.33±14.62%) (Supplemental Fig. S1d and e).

The isogenic control and the RyR-H29D hiPSC—CMs express typical sarcomeric cardiac markers

We next verified that cardiac cells derived from the variant and control lines expressed cardiac genes including components of the contractile machinery and ECC. Fold change in relative expression analysis using qPCR indicated similar potential for cardiac differentiation at the same stage, such as the cardiac ryanodine receptor type 2 (*RYR2*) (ratio of 3.95±1.65 for the RyR2-H29D vs. 1.00±0.35 for the isogenic control hiPSC—CMs, p = 0.2), myosin light chain 2 (*MYL2*) (ratio of 8.56±7.83 for the RyR2-H29D vs. 1.00±0.05 for the isogenic control hiPSC—CMs, p = 0.7) and SERCA2a (*ATP2A2*) (ratio of 1.24± 0.67 for the RyR2-H29D vs. 1.00±0.59 for the isogenic control hiPSC—CMs, p = 0.9) (Supplemental Fig. S2a). We evaluated the expression of the cardiac markers by immunocytochemistry by focusing on the presence of sarcomeres using α-actinin, cTnI and cTnT staining. Our data showed similar sarcomeric patterns by the expression of cardiac troponin I (cTnI) and T (cTnT) and α-actinin in RyR2-H29D and isogenic control hiPSC—CMs (Supplemental Fig. S2b).

Impairment of Ca^{2+}homeostasis in RyR-H29D hiPSC—CMs under physiological pacing

To assess whether the RyR2-H29D mutation affects SR Ca^{2+} handling in patient-specific hiPSC—CMs, we investigated the SR Ca^{2+} handling properties by comparing the intracellular Ca^{2+} variations in RyR2-H29D hiPSC—CMs using confocal fluorescent microscopy, compared to isogenic control hiPSC—CMs. We used hiPSC—CMs treated with the commercially-available Pluricyte medium, which has been reported to induce a more mature phenotype by improving T-tubule formation, ECC, action potential and pharmacological responses [13]. RyR2-H29D hiPSC—CMs exhibited defects in SR Ca^{2+} handling properties with higher amplitude at 1 Hz pacing (0.53±0.03 for the RyR2-H29D vs. 0.25±0.01 for the isogenic control, p<0.01) (Fig. 1a and b). RyR2-H29D hiPSC—CMs exhibited diastolic leaky events (frequency of occurrence of 1.02±0.09 Hz for the RyR2-H29D vs. 0.00±0.00 Hz for the isogenic control, p<0.01) (Fig. 1a and c). The mutant hiPSC—CMs also displayed higher Ca^{2+}-release velocity through RyR2 (rate of Ca^{2+} release of 5.38±0.59 ΔF/s for the RyR2-H29D vs. 0.81±0.04 ΔF/s for the isogenic control, p<0.01) and similar mean decay time (0.58±0.04 ms for the RyR2-H29D vs. 0.57±0.01 ms for the isogenic control, p = 0.15) (Fig. 1d and e). In addition to differences in the means of the parameter measured above, RyR2-H29D hiPSC—CMs exhibited larger variability for each of these parameters when compared to isogenic control cells. Under 0.5 Hz pacing, similar defects were observed in RyR2-H29D hiPSC—CMs (Supplemental Fig. S3a to e). We tested a second RyR2-H29D hiPSC clone (RyR2-H29D-2) to ensure that the aberrant events in RyR2-H29D cells were not clone-dependent and we employed a female healthy control (HC) hiPSC line already characterized [8] to be compared with the isogenic control hiPSC—CMs (Supplemental Fig. S4a). Under 1 Hz, the RyR2-H29D-2 hiPSC—CMs exhibited more aberrant Ca^{2+} transients and diastolic leaky events (frequency of occurrence of 0.28±0.04 Hz for the RyR2-H29D-2 vs. 0.07±0.02 Hz for the isogenic control, p<0.01) (Supplemental Fig. S4b and c).

Increased diastolic Ca^{2+} leak in RyR-H29D hiPSC—CMs

To examine whether RyR2-H29D channels are leaky in the patient-specific RyR2-H29D hiPSC—CMs, we assessed the magnitude of SR Ca^{2+}leak using tetracaine and caffeine treatments in a Na^{+} and Ca^{2+}-free solution to abolish Ca^{2+} influx from the extracellular environment. Following 1 Hz field stimulation, application of tetracaine (1 mM), a RyR2 inhibitor, caused a reduction in the Ca^{2+} baseline level in both cell groups. 50% of the RyR2-H29D hiPSC—CMs spontaneously exhibited Ca^{2+}release events while this did not occur in any of the isogenic control cells (Fig. 2a and b). However, no difference was observed in the percentage of SR Ca^{2+}leak (60.88±13.38% for the RyR2-H29D vs. 53.19±4.39% for the isogenic control, p = 0.81) (Fig. 2a and c). Application of high concentration of caffeine (30 mM) induced an exhaustive release of SR Ca^{2+} through RyR2 which reflected SR Ca^{2+} content. RyR2-H29D hiPSC—CMs showed higher release amplitude in response to caffeine (1.99±0.38 for the RyR-H29D vs. 0.66±0.23 for the isogenic control, p<0.05) (Fig. 2d and e) whereas Ca^{2+} reuptake remained unchanged between the 2 groups (Fig. 2f). The RyR2-H29D exhibited higher diastolic calcium compared to the isogenic control (0.83±0.02 for the RyR-H29D vs. 0.67±0.01 for the isogenic control, p<0.01). A unique aspect of the clinical phenotype of PMVT is that the patients do not develop arrhythmias during exercise. To evaluate if the ß-adrenergic receptor stimulation affects the SR calcium handling, we applied 1 μM of isoproterenol and high electrical pacing (2 Hz). In these stress conditions, we found an increased diastolic calcium level in the isogenic control (0.67±0.01 prior vs. 0.77± 0.02 upon isoproterenol and pacing for the isogenic control, p<0.01) but not in the RyR2-H29D hiPSC—CMs (0.83±0.02 prior vs. 0.92± 0.03 upon isoproterenol and pacing for the RyR2-H29D, p = 0.25) (Supplemental Fig. S5).

IP_3 receptors are implicated in releasing Ca^{2+}in RyR-H29D hiPSC—CMs

RyR2 and inositol 1,4,5-trisphosphate receptors (IP_3R) are the two main intracellular Ca^{2+} release channels in CMs. We tested whether IP_3R is involved in the aberrant SR Ca^{2+} release through RyR2-H29D in the RyR2-H29D hiPSC—CMs. We assessed the contribution of the IP_3R in the Ca^{2+} transients by specific pharmacological inhibition using Xestospongin C, a specific IP_3R antagonist under physiological pacing. In RyR2-H29D hiPSC—CMs, we found a decrease of the Ca^{2+} transient amplitude following application of Xestospongin C (0.48± 0.03 prior vs. 0.31±0.04 upon Xestospongin C, p<0.05) (Fig. 3a and b) with similar Ca^{2+}-release velocity (Fig. 3C). In contrast, none of the investigated properties were modified by the application of Xestospongin C in the isogenic control hiPSC—CMs (Fig. 3a, b and c), indicating that IP_3R inhibition does not affect the Ca^{2+} transient properties in control cells. Of note, application of Xestospongin C did not prevent the aberrant events in RyR2-H29D hiPSC—CMs (Fig. 3d and e). We examined whether RyR2-H29D cells differently express

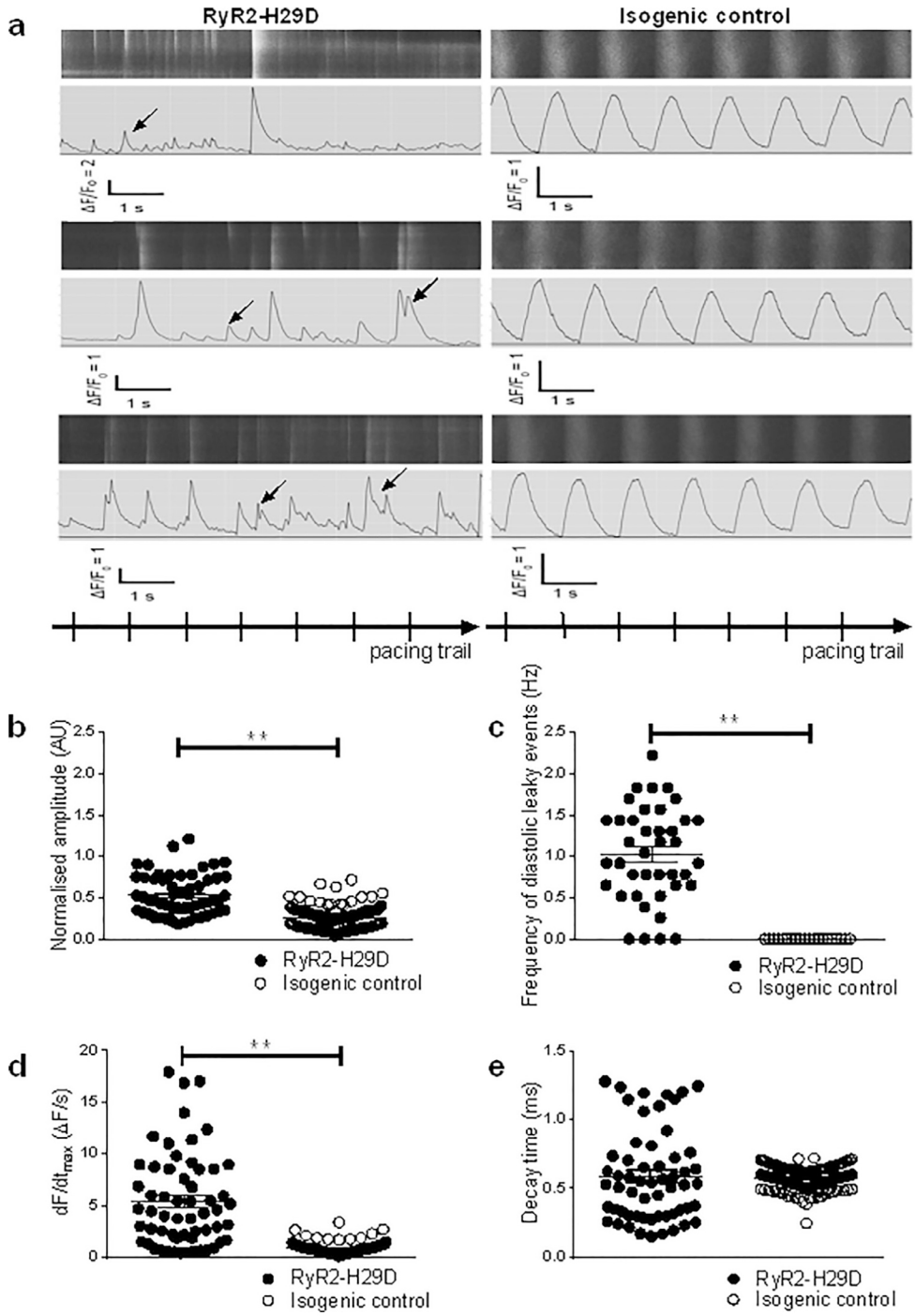

Fig. 1. Aberrant release of Ca^{2+}in RyR2-H29D hiPSC—CMs. (**a**) Display of original line-scan images of Ca^{2+} transients and corresponding tracings and pacing trail in RyR2-H29D and isogenic control hiPSC—CMs under 1 Hz pacing (20 V and 5 ms duration). Additional and aberrant Ca^{2+} release events are shown with the arrows in RyR2-H29D hiPSC—CMs. Note a different vertical scale bar between RyR2-H29D and isogenic controls (**b**) Normalized Ca^{2+}-transient amplitude in RyR2-H29D hiPSC—CMs (black dots plot) and isogenic control hiPSC—CMs (white dots plot) under 1 Hz pacing. **(c)** Frequency of occurrence of diastolic leaky events in RyR2-H29D and isogenic control hiPSC—CMs. **(d)** Rate of RyR2 Ca^{2+} release (dF/dt_{max} in $\Delta F/s$) in RyR2-H29D and isogenic control hiPSC—CMs. **(e)** Decay time in RyR2-H29D and isogenic control hiPSC—CMs. The number of experiments varies from 24 to 146 cells for each scatter plot from 3 independent biological replicates. Data are presented as mean ± SEM. Significance was calculated by Mann-Whitney test. **, $p < 0.01$.

RyR2 and IP_3R at the protein level and found no difference compared to the isogenic control cells (Supplemental Fig. S6a, b and c).

RyR2-H29D leads to macromolecular complex post-translational remodeling

We next tested whether the RyR2-H29D mutation expressed in the RyR2-H29D hiPSC—CMs causes post-translational modifications of the RyR2 macromolecular complex. To that end, we explored RyR2 biochemical properties by co-immunoprecipitation RyR2 in hiPSC—CM lysates. Under non-stress conditions, we examined the RyR2 PKA and CaMKII-phosphorylation level, oxidation, cysteine S-nitrosylation and the amount of calstabin2 bound to the channel as these post-translational modifications have been identified to remodel RyR2.

We found that the RyR2-H29D hiPSC—CMs exhibit higher PKA-phosphorylated RyR2 at Ser 2809 (3.70±0.20 for the RyR2-H29D vs. 0.10±0.10 for the isogenic control, $p<0.01$) associated with oxidation

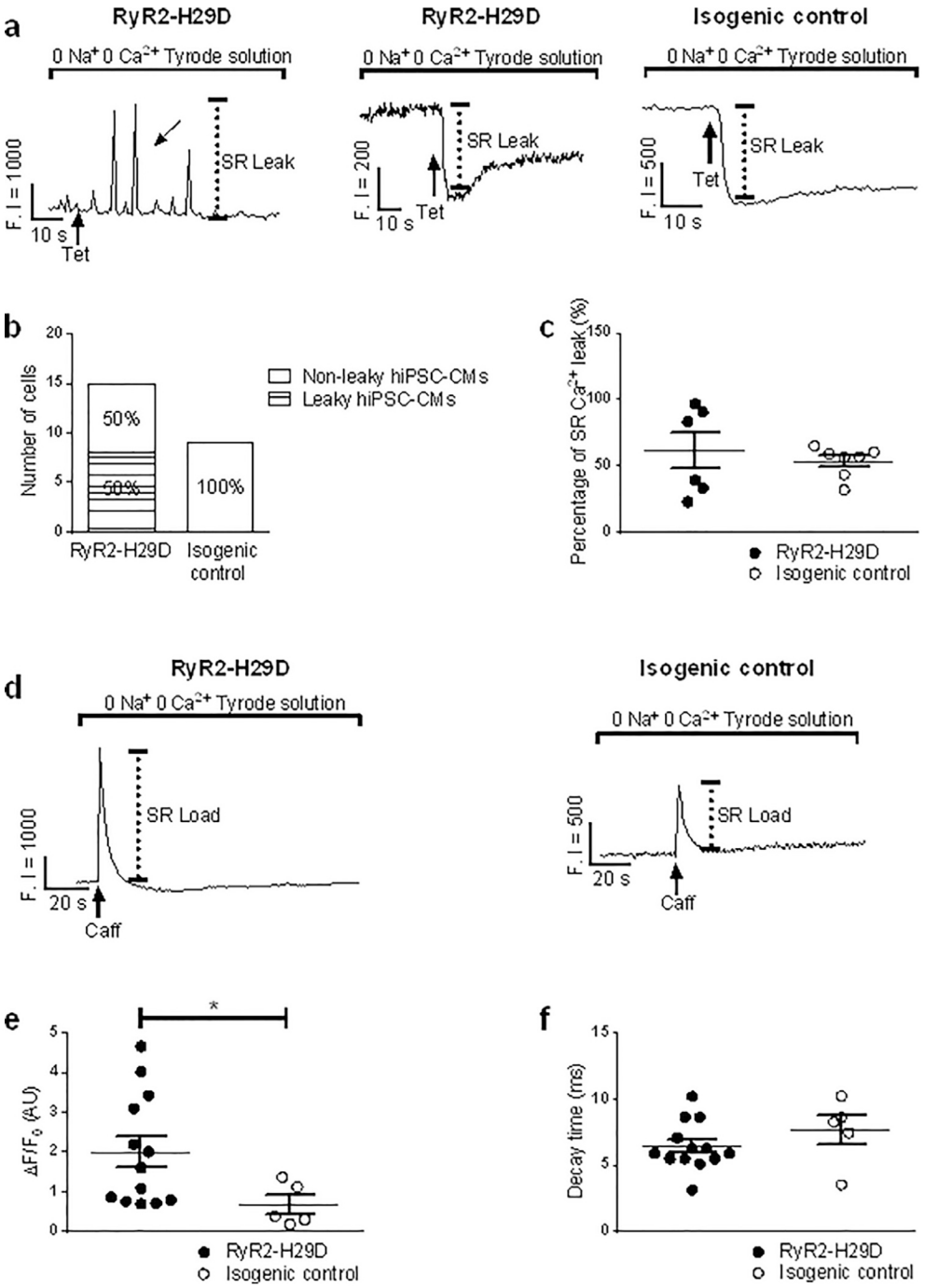

Fig. 2. Altered Ca^{2+} homeostasis in RyR2-H29D hiPSC—CMs. (a) Representative traces of cytosolic Ca^{2+} fluorescence in RyR2-H29D and isogenic control hiPSC—CMs in 0 Na^+, 0 Ca^{2+} solutions containing 1 mM Tetracaine (Tet). Spontaneous Ca^{2+} oscillations (marked by arrows) were present in RyR2-H29D hiPSC—CMs in Na^+ and Ca^{2+}-free conditions. (**b**) Number of cells exhibiting SR Ca^{2+} leak in RyR2-H29D and isogenic control hiPSC—CMs. **(c)** Percentage of SR Ca^{2+} leak in RyR2-H29D hiPSC—CMs (black dots plot) and isogenic control hiPSC—CMs (white dots plot). **(d)** Representative traces of cytosolic Ca^{2+} fluorescence in RyR2-H29D and isogenic control hiPSC—CMs in 0 Na^+, 0 Ca^{2+} solutions upon 30 mM caffeine (Caff). **(e)** Amplitude of SR Ca^{2+} load in RyR2-H29D and isogenic control hiPSC—CMs. **(f)** Decay phase of the SR Ca^{2+} load in RyR2-H29D and isogenic control hiPSC—CMs. The number of experiments varies from 5 to 16 cells for each scatter plot from 3 independent biological replicates. Beside the Fig. 2B, data are presented as mean ± SEM. Significance was calculated by Mann-Whitney test. *, $p < 0.05$.

and Cys-S-nitrosylation compared to the isogenic control cells (Fig. 4a, b, d and e). There was no change in CaMKII-phosphorylated RyR2 at Ser 2815 (Fig. 4a and c). Calstabin2 binding to RyR2 was also largely reduced in RyR2-H29D hiPSC—CMs (0.50±0.10 for the RyR2-H29D vs. 4.00±0.20 for the isogenic control, $p<0.01$) (Fig. 4a and e). No particular RyR2 remodeling was observed in the isogenic control hiPSC—CMs harbouring RyR2 channels with the corrected amino acid (Fig. 4a-e). We further examined the RyR2 remodeling using previously characterized gender-matched healthy control and CPVT RyR2-D3638A hiPSC—CMs previously characterized [8]. Comparable to the isogenic control hiPSC—CMs, both the healthy control and CPVT hiPSC—CMs exhibited no RyR2 remodeling. However, under stress conditions using β-adrenergic stimulation with isoproterenol, RyR2 was PKA-phosphorylated, oxidized, S-nitrosylated and calstabin2 depleted in CPVT and healthy control hiPSC—CMs (Supplemental Fig. S6d).

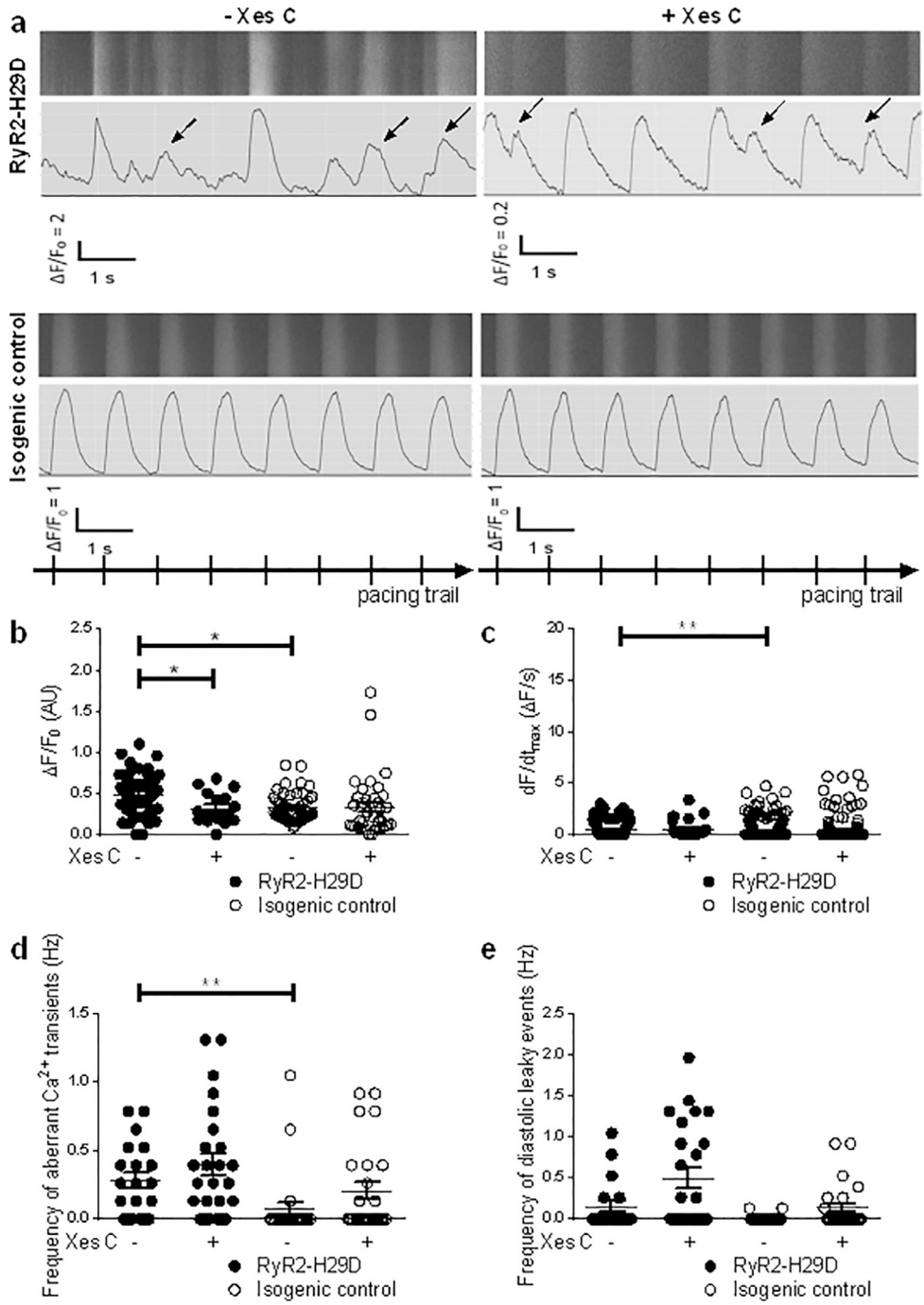

Fig. 3. IP_3 receptors are further implicated in Ca^{2+}release in RyR2-H29D hiPSC—CMs. (a) Representative traces of cytosolic Ca^{2+} fluorescence in RyR2-H29D and isogenic control hiPSC—CMs in absence and presence of 10 μM of Xestospongin C (Xes C). **(b)** Maximal Ca^{2+}-transient amplitude in RyR2-H29D hiPSC—CMs (black dots plot) and isogenic control hiPSC—CMs (white dots plot) under 1 Hz pacing and ± 10 μM of Xes C. **(c)** Rate of RyR2 Ca^{2+} release (dF/dt_{max} in ΔF / s) in RyR2-H29D hiPSC—CMs and isogenic control under 1 Hz pacing and ± 10 μM of Xes C. **(d)** Frequency of aberrant Ca^{2+}-transients in RyR2-H29D hiPSC—CMs and isogenic control hiPSC—CMs under 1 Hz pacing and ± 10 μM of Xes C. **(e)** Frequency of occurrence of diastolic leaky events in RyR2-H29D hiPSC—CMs and isogenic control hiPSC—CMs under 1 Hz pacing and ± 10 μM of Xes C. The number of experiments varies from 20 to 303 cells for each scatter plot from 3 independent biological replicates. Data are presented as mean ± SEM. Significance was calculated by Kruskal-Wallis test. *, $p < 0.05$.

Abnormal electrical properties in RyR-H29D hiPSC—CMs

We investigated the effect of the H29D mutation on the electrophysiological properties of cardiomyocytes under physiological pacing (1 Hz). The RyR2-H29D hiPSC—CMs exhibited decrease of the AP duration at 50% (APD_{50}) and 90% of repolarization (APD90) (mean APD_{50} of 122.90±17.77 ms for the RyR2-H29D vs. 226.60±40.30 ms for the isogenic control, $p<0.01$ and mean APD_{90} of 219.50±23.52 ms for the RyR2-H29D vs. 340.30±45.21 ms for the isogenic control, $p<0.01$) suggesting a short AP in the RyR2-H29D cells (Fig. 5a-c). The APD90/APD50 ratio suggested that we obtained both, atrial- and ventricular-like cells, with no difference between the RyR2-H29D hiPSC—CMs and the isogenic control hiPSC—CMs (ratio of 2.15±0.19 for the RyR2-H29D vs. 2.17±0.51 for the isogenic control, $p = 0.17$) (Fig. 5d). The RyR2-H29D hiPSC—CMs displayed similar AP amplitude and depolarization velocity compared to the isogenic control cells (Fig. 5a, b, e and f). We investigated whether the RyR2-H29D mutation has arrhythmogenic consequences. By comparing the number of DADs leading to short-coupled premature ventricular contractions (PVCs) and PMVT [4], we found that RyR2-H29D hiPSC—CMs

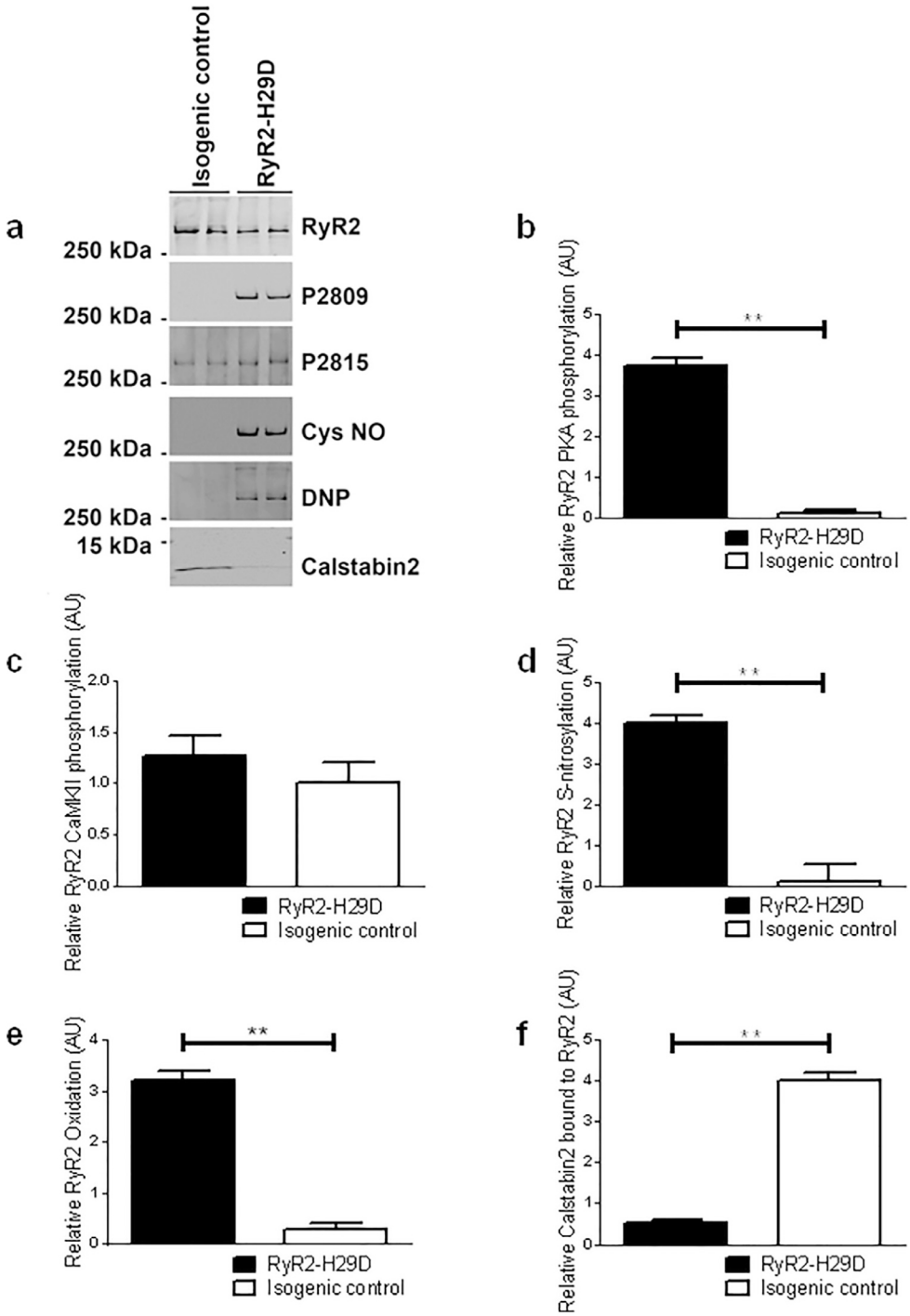

Fig. 4. Post-translational modifications associated with the RyR2-H29D mutation. (a) Immunoblots of the RyR2 co-immunoprecipitation showing the level of RyR2 PKA-phosphorylation at Ser2809 (P2809), CaMKII phosphorylation at Ser2815 (P2815), S-nitrosylation of cysteines (Cys-NO), cysteine (DNP) and calstabin2 (FKBP12.6) binding in isogenic control and RyR2-H29D hiPSC—CMs. (b) Relative RyR2 PKA-phosphorylation level at Ser2809 in RyR2-H29D (black bars) and isogenic control (white bars) hiPSC—CMs. (c) Relative RyR2 CaMKII-phosphorylation level at Ser2815 in RyR2-H29D and isogenic control hiPSC—CMs. (d) Relative RyR2 S-nitrosylation level in RyR2-H29D and isogenic control hiPSC—CMs. (e) Relative RyR2 oxidation level in RyR2-H29D and isogenic control hiPSC—CMs. (f) Relative Calstabin2 amount bound to RyR2 in RyR2-H29D and isogenic control hiPSC—CMs. The results are based on 3 independent biological replicates. Data are presented as mean ± SEM. Significance was calculated by Mann-Whitney test. **, $p < 0.01$.

exhibited DADs by 40%. No DADs were seen in the isogenic control hiPSC—CMs (Fig. 5a-g).

Aberrant contractile and relaxing properties in RyR-H29D hiPSC—CMs

We tested whether the RyR2-H29D hiPSC—CMs differentiated through a 2D cardiac monolayer syncytium could display evidences of aberrant contractile activity in the dish. We assessed video-capture on a hiPSC—CM 2D monolayer spontaneously beating at 37 °C. We compared the RyR2-H29D and isogenic control monolayers. We observed a lower beat rate (168.10±5.13 bpm for the RyR2-H29D vs. 185.40±5.38 bpm for the isogenic control, $p<0.01$) and no difference in the average amplitude and contraction time (Fig. 6a, b, c and d). However, a higher relaxation time (118.60±5.51 ms for the RyR2-H29D vs. 99.35±4.20 ms for the isogenic control, $p<0.01$) and resting time (149.60±8.06 ms for the RyR2-H29D vs. 132.40± 12.68 ms for the isogenic control, $p<0.01$) and lower homogeneity were observed in the cardiac 2D monolayer composed of RyR2-

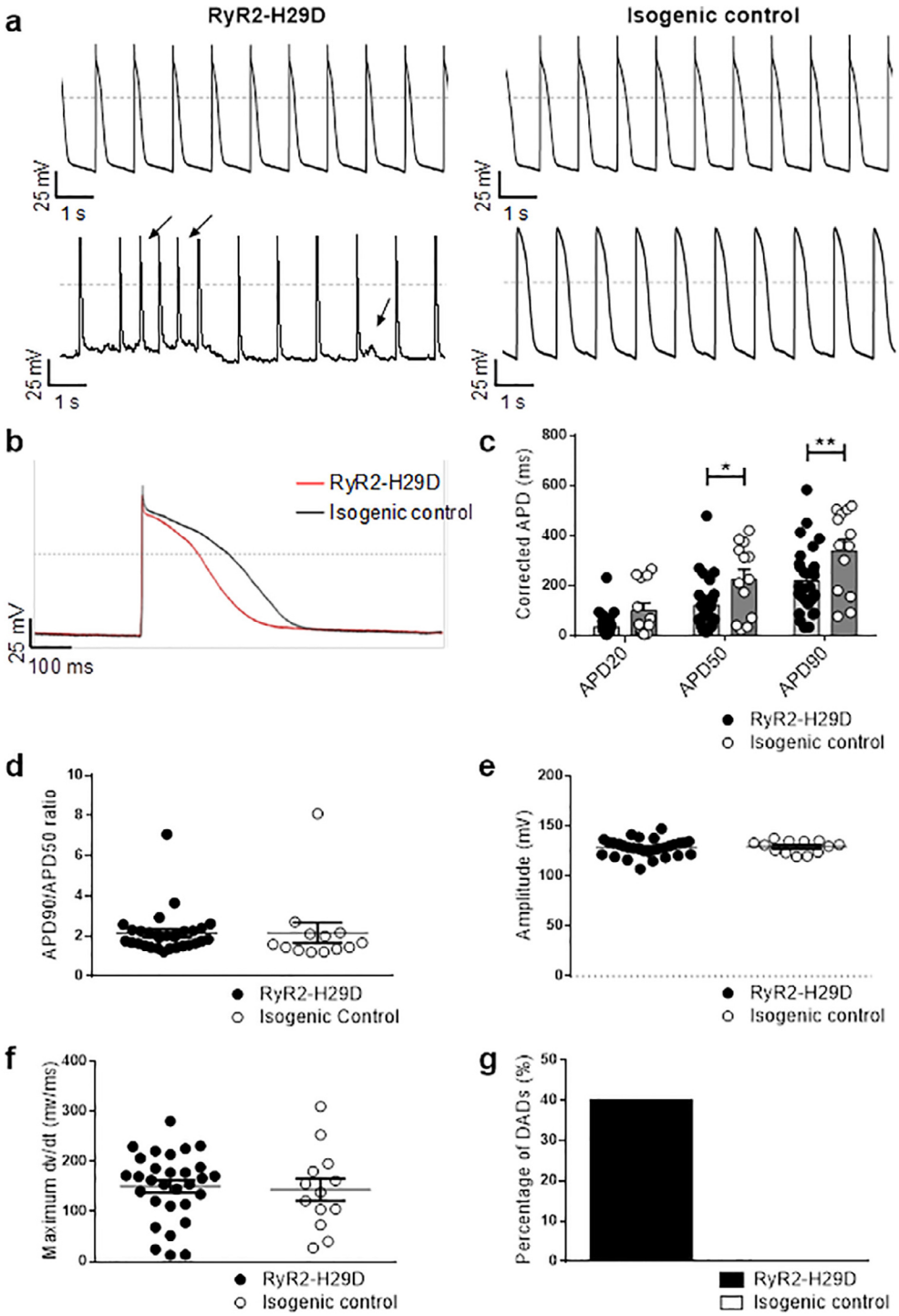

Fig. 5. Action potentials recorded from RyR2-H29D and isogenic control hiPSC—CMs. (a-b) Example of action potential (AP) from RyR2-H29D (left) and isogenic control (right) hiPSC—CMs at 1 Hz using patch-clamp technique. Additional and aberrant depolarizations are shown with the arrows in RyR2-H29D hiPSC—CMs. **(c)** Bar graphs showing the corrected AP duration in RyR2-H29D hiPSC—CMs (black dots plot) and isogenic control hiPSC—CMs (white dots plot) at 1 Hz. Corrected AP was the result of artificially lowering the maximum diastolic potential to −80 mV. **(d)** Scatter plots showing the APD90/APD50 ratio in RyR2-H29D hiPSC—CMs (black dots plot) and isogenic control hiPSC—CMs (white dots plot) at 1 Hz. **(e)** Scatter plots showing the AP amplitude in RyR2-H29D hiPSC—CMs and isogenic control hiPSC—CMs at 1 Hz. **(f)** Scatter plots showing the maximum depolarization speed (dv/dt) in RyR2-H29D hiPSC—CMs and isogenic control hiPSC—CMs at 1 Hz. **(g)** Bar graphs showing the percentage of delay afterdepolarizations (DADs) in RyR2-H29D (black bars) and isogenic control (white bars) hiPSC—CMs at 1 Hz. The number of experiments varies from 13 to 30 cells for each scatter plot from 3 independent biological replicates. Data are presented as mean ± SEM. Significance was calculated by Mann-Whitney test. * $p < 0.05$; ** $p < 0.01$.

H29D hiPSC—CMs (Fig. 6a, e, f and g and supplemental movies S1 and S2).

3D in-silico modeling reveals the impact of the RyR-H29D mutation

The H29 residue is conserved in the amino-acid sequence of RyR2 from several species while the mutation brings a negative charge at position 29 [4]. Using the recent and available 3D structures of RyR2 and RyR1 homotetramers [14, 15], we analysed the potential impact of the RyR2-H29D mutation on the RyR2 structure/function relationship to further understand how the mutation could lead to SR calcium leak and RyR2 post-translational remodeling. By using 3D *in-silico* modeling, we determined that H29 interacts with a loop containing the D378 and K380 residues from a neighbouring monomer

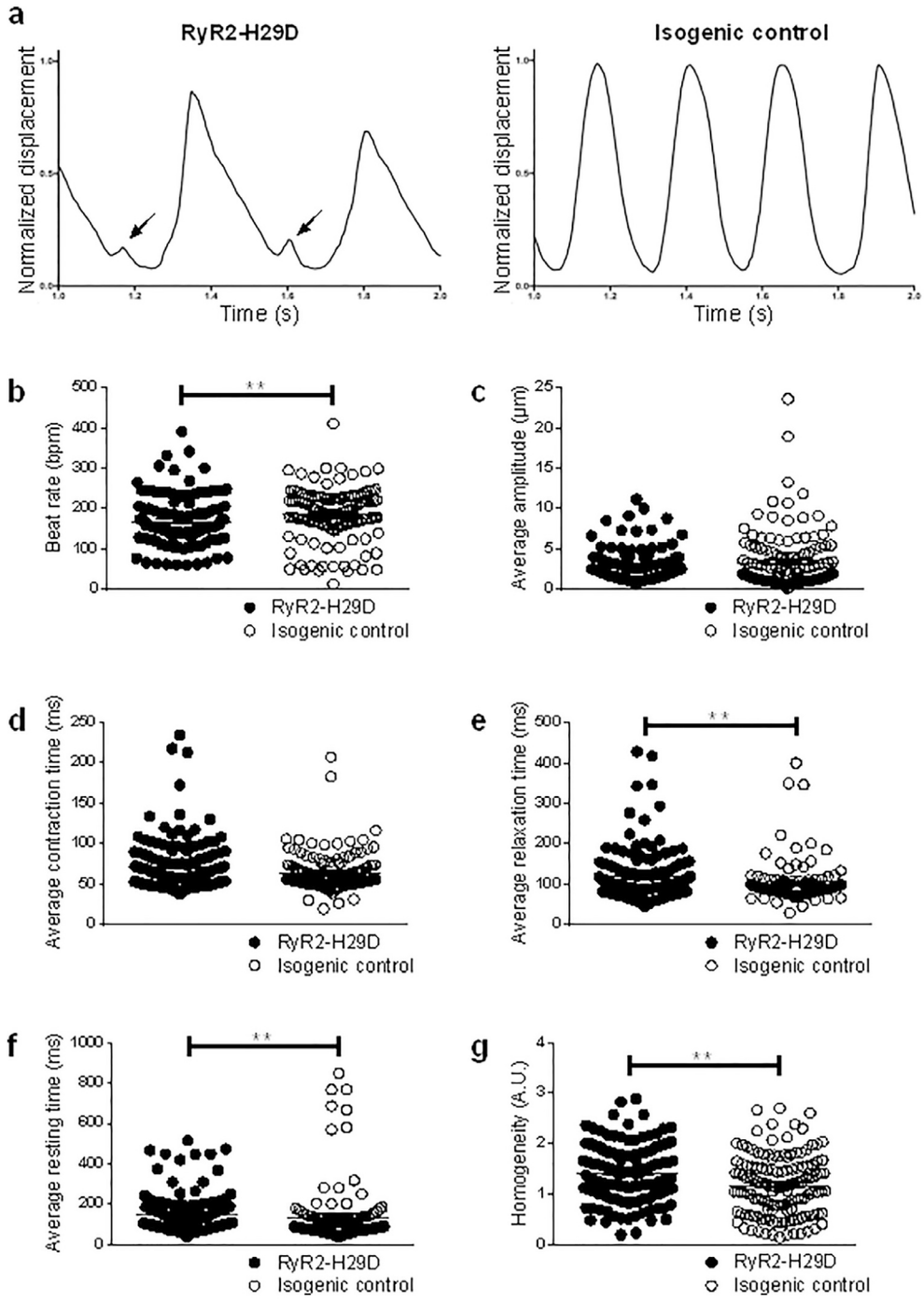

Fig. 6. Aberrant contractile properties through video-image-based analysis (i.e., auxotonic contraction) in RyR2-H29D hiPSC—CMs. (a) Representative traces of contractile parameters in RyR2-H29D and isogenic control hiPSC—CMs. Aberrant contraction oscillations (marked by arrows) were present in RyR2-H29D, but not in isogenic control hiPSC—CMs. (**b**) Beat rate in RyR2-H29D hiPSC—CMs (black dots plot) and isogenic control hiPSC—CMs (white dots plot). **(c)** Average amplitude in RyR2-H29D hiPSC—CMs and isogenic control. **(d)** Average contraction time in RyR2-H29D hiPSC—CMs and isogenic control hiPSC—CMs. **(e)** Average relaxation time in RyR2-H29D hiPSC—CMs and isogenic control hiPSC—CMs. **(f)** Average resting time in RyR2-H29D hiPSC—CMs and isogenic control hiPSC—CMs. **(g)** Homogeneity in RyR2-H29D hiPSC—CMs and isogenic control hiPSC—CMs. The number of experiments varies from 135 to 140 videos for each scatter plot from 3 independent biological replicates. Data are presented as mean ± SEM. Significance was calculated by Mann-Whitney test. **, $p < 0.01$.

(Supplemental Fig. S7a). The RyR2-H29D mutation may change the balance of charged residues at this interface between the monomers forming the entrance of the tetrameric channel. A large part of the D378 loop, namely a fragment 379–386 with the sequence VKSVRMGS is not resolved in the structure. In addition, the structure of a loop 2803–2818 (RTRRISQTSQVSVD) with phosphorylated S2809 remains unknown. The S2809 loop is far from H29 of the same monomer (more than 120 Å). However, contact between S2809 and H29 may be possible due to the subunit movements (Supplemental Fig. S7b).

Discussion

In this study, we used hiPSC—CMs to provide a patient-specific model of short-coupled PMVT at rest associated with a RyR2 point mutation (Central Illustration in Fig. 7). Previously, we showed that

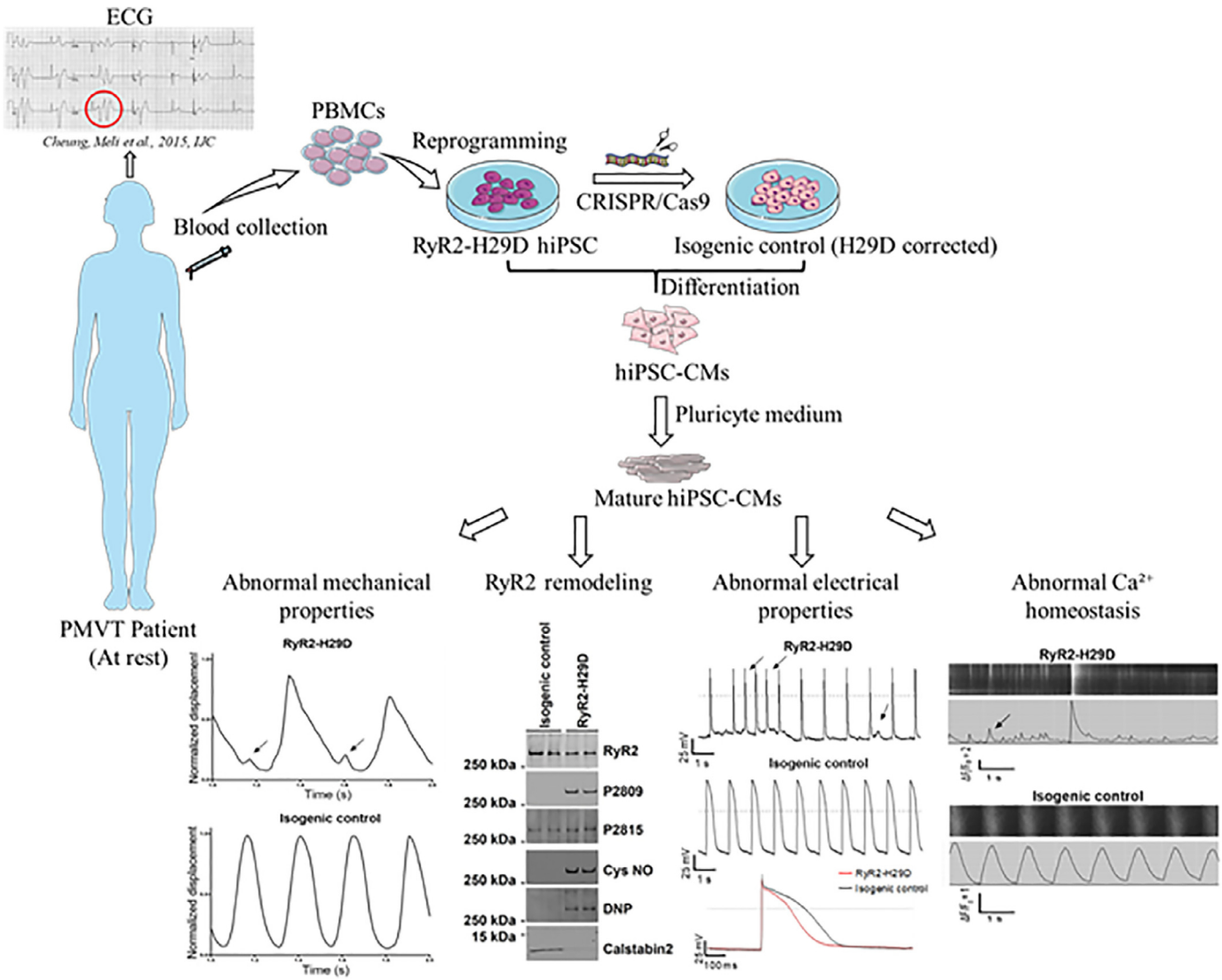

Fig. 7. Recapitulative scheme of the performed study from the PMVT proband to the dish. Recapitulative scheme illustrating the RyR2-H29D hiPSC generated from the PMVT proband blood sample. Some isogenic control hiPSC were generated by correcting the single-point mutation using CRISPR/Cas9 technology. The RyR2-H29D and isogenic control hiPSC—CMs were differentiated. The RyR2-H29D hiPSC—CMs exhibited abnormal calcium homeostasis, aberrant electrical and mechanical properties and RyR2 remodeling under non-stress conditions which were abolished in the isogenic control hiPSC—CMs.

the recombinant RyR2-H29D mutant expressed in a heterologous system causes a gain-of-function with increased open probability, opening frequency and sensitivity to low diastolic calcium at rest [4]. Here, using patient-specific hiPSC—CMs, we found that this single-point mutation RyR2-H29D is associated with several key properties: 1) aberrant SR Ca^{2+} leak under physiological pacing, 2) pro-arrhythmic electrical phenotypes, 3) impaired and asynchronous contractile properties and 4) aberrant RyR2 post-translational modifications, all under non-stress conditions. The presence of these findings at rest recapitulate the unique phenotype of PMVT occurring at rest in our study patients with the RyR2-H29D mutation. Furthermore, correction of the H29D variant by a single residue conversion in patient-specific hiPSC—CMs was sufficient to prevent these abnormalities, which provides evidence that short-coupled PMVT at rest can be associated with RyR2 dysfunction.

At day 15, we found no difference in cardiac specification between RyR2-H29D and control hiPSC—CMs. At day 30, the expressed cardiac markers were also similar. These data excluded that the RyR2 mutation impacts the early cardiac development. We observed that RyR2-H29D hiPSC—CMs have shorter AP and more DADs compared to the isogenic control. Shorter AP and spatial heterogeneity of AP duration have been reported in a case of short-coupled variant of TdP [16] while heterogeneity in repolarization in a TdP dog model has been observed [17]. The DADs likely trigger short-coupled PVCs and PMVT as we previously claimed [4]. Our previous findings revealed that the RyR2-H29D mutation is a gain-of-function mutation causing Ca^{2+} leak [4]. The present study supports these results. In addition, we found that RyR2-H29D hiPSC—CMs have higher Ca^{2+}release upon caffeine and higher diastolic calcium which would suggest higher SR Ca^{2+} content in cells expressing the RyR2-H29D mutant channels compared to isogenic control hiPSC—CMs. While others have demonstrated lower SR Ca^{2+} content associated with Ca^{2+} leak through RyR2 in CPVT syndrome [18], we demonstrated that the RyR2-D3638A CPVT mutant, although leaky under stress, does not affect SR Ca^{2+} content [8]. The impact of SR Ca^{2+} content on RyR2-H29D-mediated arrhythmogenesis remains to be determined. However, we could speculate that the elevated intracellular calcium concentration activates the inward current (I_{NCX}) triggering DADs. Of note, we observed that the RyR2-H29D hiPSC—CMs does not respond to stress and maintain similar diastolic calcium level when compared to isogenic control hiPSC—CMs. These results agree with the RyR2-H29D mutant molecular remodeling showing high PKA phosphorylation at

Ser2809 at rest. This suggests that, somehow, the RyR2-H29D mutant channels are not impacted by the ß-adrenergic receptor stimulation because they are already PKA-phosphorylated at rest.

The patients with PMVT experience asynchronous ventricular contractions and short-coupled PVCs. We found that PMVT hiPSC—CMs were characterized by bradycardia and slower relaxation, higher resting time and asynchronous cycles of contraction. We observed that the CMs harboring the RyR2-H29D mutant channels, displayed more heterogeneous and asynchronous contractions. To compare, the isogenic control hiPSC—CMs carrying RyR2-WT channels exhibit synchronous contraction/relaxation cycles which demonstrate the deleterious impact of the single-point RyR2-H29D on the patient-specific cardiac contractile properties. These PMVT hiPSC—CM findings recapitulate the asynchronous ventricular contractions observed in PMVT patients [16, 17] and bradycardia known to trigger PMVT [19]. Our results indicated a high spontaneous beat rate (>160 bpm) with the PMVT hiPSC—CMs. This is reminiscent of child high heart rate [20]. Moreover, the Pluricyte medium we employed contains T3 hormone known to increase heart rate, cardiac contractility and cardiac output [21].

In two heart failure models, increased expression and altered localization of IP_3 receptors have been associated with arrhythmias [22, 23]. Whether or not there is cross-talk between RyR2 and IP_3R2 in cardiomyocytes in pathophysiological conditions is unclear [24]. Nakayama et al. had shown that the IP_3R-dependent Ca^{2+} release at the T-tubule-SR junction could stimulate SR Ca^{2+} leak through RyR2 [25]. Itzhaki et al. demonstrated that immature hiPSC—CMs exhibit Ca^{2+} release via IP_3R to modulate the spontaneous Ca^{2+} transients [26]. With a more mature degree through Pluricyte medium application, we observed that RyR2-H29D hiPSC—CMs displayed weaker peak Ca^{2+} transients upon pharmacological IP_3R inhibition under physiological pacing, which was not seen with isogenic control hiPSC—CMs. Of note, the inhibition of IP_3R did not suppress the occurrence of abnormal release of Ca^{2+} in the RyR2-H29D hiPSC—CMs. We found no difference in RyR and IP_3R protein expression between the 2 groups of hiPSC—CMs. Therefore, these results suggest that RyR2-H29D enhances the contribution of IP_3R to ECC that exacerbates abnormal Ca^{2+} release in RyR2-H29D hiPSC—CMs. Furthermore, it was shown that PKA phosphorylation of the IP_3R increases Ca^{2+} release at low IP_3 concentrations [27]. In the RyR2-H29D hiPSC—CMs, the PKA-phosphorylated RyR2-H29D channels may enhance the IP_3R activity. The Ca^{2+} release through IP_3R may contribute to arrhythmogenesis. More experiments will be needed to further evaluate their contribution to PMVT at rest.

We found that the RyR2-H29D mutation confers significant alterations of the RyR2 macromolecular complex. In RyR2-H29D hiPSC—CMs, RyR2 PKA-hyperphosphorylation at Ser2809 as well as oxidation, S-nitrosylation and depletion of calstabin2 were seen. The RyR2 CaMKII-phosphorylation at Ser2815 was unchanged. These post-translational modifications were not present in RyR2-WT isogenic controls, gender-matched healthy controls, or CPVT RyR2-D3638A hiPSC—CMs. The post-translational RyR2 modifications seen with RyR2-H29D hiPSC—CMs were similar to those seen in healthy control and CPVT hiPSC—CMs under conditions of ß-adrenergic receptor activation (i.e., stress conditions). Furthermore, correction of the RyR2-H29D variant in isogenic control cells fully prevents these post-translational modifications. These findings suggest that PMVT hiPSC—CMs harbouring RyR2-H29D in non-stress conditions can behave like CPVT CMs with increased aberrant arrhythmias under stress conditions [28]. Moreover, the application of isoproterenol did not affect the diastolic calcium level in RyR2-H29D hiPSC—CMs. Thus, PKA hyperphosphorylation of the RyR2-H29D channel may explain the relative ineffectiveness of ß-blocker therapy for short-coupled PMVT compared to CPVT. Park et al. [29] and Di Pasquale et al. [30] have both shown that CaMKII phosphorylation at Ser2814 may contribute to SR Ca^{2+} leak in the CPVT hiPSC—CMs, meaning that CaMKII inhibitors may be of high interest to prevent CPVT. This therapeutic strategy does not seem to be right for the PMVT RyR2-H29D mutant channel as the RyR2 CaMKII-phosphorylation level was unaffected. In the clinical treatment of our study patients with RyR2-H29D mutations, catheter ablation of PVCs was the most effective way for preventing future arrhythmias.

Overall, the results presented here differ from results previously obtained with recombinant human RyR2-H29D expressed in HEK293 cells [4]. In HEK293 cells, the depletion of calstabin2 was less pronounced compared to the results obtained in RyR2-H29D hiPSC—CMs. In this regard, patient-specific RyR2-H29D hiPSC—CMs likely constitute a more accurate and relevant model to decipher the underlying molecular mechanisms leading to RyR2-H29D induced-short coupled PMVT. Specifically, hiPSC—CMs are mature enough to reveal post-tranlational modifications associated with aberrant functional properties of the RyR2-H29D mutant channels.

Our results contrast with those published by Xiao et al. describing no consequence of the recombinant RyR2-H29D mutant compared to RyR2-WT when expressed in HEK cells [31]. Using the 3D RyR2 and RyR1 available structures, we performed 3D *in-silico* protein modeling to investigate the impact of the RyR2-H29D mutation on the structure/function relationship. Our findings indicate that the H29 of one monomer is in close proximity to a loop containing the D378 and K380 residues from a neighbouring monomer and therefore, they likely interact. These residues are contained in the amino terminal domain which is composed of several armadillo domains and α-helix pairs. The RyR2-H29D mutation may change the balance of charged residues (i.e., from a positively charged to negatively charged residue) at this interface between the monomers forming the entrance of the tetrameric channel. Unfortunately, the unresolved sequence of the fragment VKSVRMGS comprised between 379 and 386 cannot provide further details. The sequence containing D378 and K380 residues is known to be a RyR2 hot-spot region sensitive for mutations associated with CPVT [1]. The structure of a loop 2803–2818 (RTRRISQTSQVSVD) with phosphorylated S2809 is also unknown. Despite the large distance (120 Å) between the S2809 loop and H29 from one monomer, possible contacts may also exist between S2809 and H29 due to the subunit movements of two monomers. Such interaction may explain the unexpected PKA-hyperphosphorylated of residue S2809 associated with the PMVT RyR2-H29D.

Notably, the RyR2-H29D mutation does not lie among the 4 hot-spots regions in RyR2 for mutations associated with CPVT and ARVC. It also does not parallel RyR1 hot-spot regions for malignant hyperthermia [32]. Recently, other PMVT and torsades de pointe-related mutations on RyR2 have been reported [33, 34] and like RyR2-H29D, the RyR2 M995V mutation associated with short coupled PMVT also does not lie within the RyR2 hot-spot regions. Therefore, the atypical locations of the RyR2-H29D and RyR2 M995V mutations likely account for the unique phenotypic expression of short-coupled PMVT at rest instead of CPVT or ARVC [35, 36].

Our study adds to the growing body of evidence that RyR2 mutations can be associated with inherited forms of arrhythmias occurring at rest and not during exertion or exercise. Our hiPSC—CM model of short coupled PMVT provides insights into abnormal RyR2 behavior that may help guide mechanism-specific therapy. Although early descriptions of the entity of short-coupled torsades de pointe identified verapamil as the therapy of choice for arrhythmia suppression [37], it is possible that treatment of RyR2 variant-associated PMVT with RyR2-targeted therapy such as flecainide [38] and Rycal compounds [8] would be beneficial. Further study on the electrophysiological response of RyR2-H29D hiPSC—CMs to different pharmacological therapies would help shed further light on the clinical implications of our findings.

In a patient-specific hiPSC—CM model of short-coupled PMVT at rest associated with the RyR2-H29D point mutation, we found that abnormal RyR2 function can lead to significant abnormalities in

calcium homeostasis and molecular modifications under non-stress conditions. It suggests that RyR2 screening should not be restricted only to patients who present with arrhythmias during stress and exercise. Our research study focused on modeling the short-coupled PMVT at rest diagnosed in 1 patient carrying the RyR2-H29D mutation. Unfortunately, the mother of our proband carrying the same mutation died of non-cardiac reasons and we did not have access to other family members that live in India. By using patient-derived cardiomyocytes, and isogenic cardiomyocytes that differ only at the single RyR2 variant, the phenotypes for the mutant cells that we describe are perhaps the best evidence yet presented for a causal link for a RyR2 variant and short-coupled PMVT. The data strongly support hiPSC—CMs as tools for disease modeling.

Contributors

YS and MS performed the experiments on the hiPSC—CMs and statistical analyses. RK, EY, TZ performed the experiments on the hiPSC and CRISPR/Cas9. FJ performed the experiments on cardiac differentiation and flow cytometry. AB, SR, AM, OC performed the experiments on calcium imaging, patch-clamp, biochemistry and statistical analyses. AK performed the 3D in silico protein modeling. BL and JC provided the clinical data and medical expertise. YS and ACM wrote the manuscript. JLP, ARM, JC, SC, TE, AL and ACM designed the study, interpreted the data and provided edits of the manuscript. All authors provided critical review of the manuscript and approved its submission.

Declaration of interests

ARM is a board member and owns shares in ARMGO Pharma Inc., which is targeting RyR channels for therapeutic purposes. All authors have nothing else to disclose. All authors read and approve the final version of the manuscript, and ensure it is the case.

Acknowledgments

We thank the “Montpellier Ressources Imagerie” (MRI) platform (https://www.mri.cnrs.fr/fr/).

Funding

This work was supported by grants of the French Muscular Dystrophy Association (AFM; project 16073, MNM2 2012 and 20225), the “Fondation de la Recherche Médicale” (FRM; SPF20130526710), the “Institut National pour la Santé et la Recherche Médicale” (INSERM), the National Institutes of Health (ARM; R01 HL145473) and the New York State Department of Health (NYSTEM C029156). The funders had no role in study design, data of collection, data analysis, interpretation or writing of the report.

References

[1] Meli AC, Refaat MM, Dura M, Reiken S, Wronska A, Wojciak J, et al. A novel ryanodine receptor mutation linked to sudden death increases sensitivity to cytosolic calcium. Circ Res 2011;109(3):281–90.

[2] Priori SG, Napolitano C, Tiso N, Memmi M, Vignati G, Bloise R, et al. Mutations in the cardiac ryanodine receptor gene (hRyR2) underlie catecholaminergic polymorphic ventricular tachycardia. Circulation 2001;103(2):196–200.

[3] Laitinen PJ, Brown KM, Piippo K, Swan H, Devaney JM, Brahmbhatt B, et al. Mutations of the cardiac ryanodine receptor (RyR2) gene in familial polymorphic ventricular tachycardia. Circulation 2001;103(4):485–90.

[4] Cheung JW, Meli AC, Xie W, Mittal S, Reiken S, Wronska A, et al. Short-coupled polymorphic ventricular tachycardia at rest linked to a novel ryanodine receptor (RyR2) mutation: leaky RyR2 channels under non-stress conditions. Int. J. Cardiol. 2015;180:228–36.

[5] Fujii Y, Itoh H, Ohno S, Murayama T, Kurebayashi N, Aoki H, et al. A type 2 ryanodine receptor variant associated with reduced Ca(2+) release and short-coupled torsades de pointes ventricular arrhythmia. Heart Rhythm 2017;14(1):98–107.

[6] Charpentier F, Bourge A, Merot J. Mouse models of SCN5A-related cardiac arrhythmias. Prog Biophys Mol Biol 2008;98(2–3):230–7.

[7] Acimovic I, Vilotic A, Pesl M, Lacampagne A, Dvorak P, Rotrekl V, et al. Human pluripotent stem cell-derived cardiomyocytes as research and therapeutic tools. Biomed Res Int 2014;2014:512831.

[8] Acimovic I, Refaat MM, Moreau A, Salykin A, Reiken S, Sleiman Y, et al. Post-Translational Modifications and Diastolic Calcium Leak Associated to the Novel RyR2-D3638A Mutation Lead to CPVT in Patient-Specific hiPSC-Derived Cardiomyocytes. J Clin Med 2018;7(11).

[9] Labun K, Montague TG, Gagnon JA, Thyme SB, Valen E. CHOPCHOP v2: a web tool for the next generation of CRISPR genome engineering. Nucleic Acids Res. 2016;44(W1):W272–W6.

[10] Hsu PD, Scott DA, Weinstein JA, Ran FA, Konermann S, Agarwala V, et al. DNA targeting specificity of RNA-guided Cas9 nucleases. Nat. Biotechnol. 2013;31(9):827–32.

[11] Tohyama S, Hattori F, Sano M, Hishiki T, Nagahata Y, Matsuura T, et al. Distinct metabolic flow enables large-scale purification of mouse and human pluripotent stem cell-derived cardiomyocytes. Cell Stem Cell 2013;12(1):127–37.

[12] Lian X, Zhang J, Azarin SM, Zhu K, Hazeltine LB, Bao X, et al. Directed cardiomyocyte differentiation from human pluripotent stem cells by modulating Wnt/beta-catenin signaling under fully defined conditions. Nat Protoc 2013;8(1):162–75.

[13] Ribeiro MC, Tertoolen LG, Guadix JA, Bellin M, Kosmidis G, D'Aniello C, et al. Functional maturation of human pluripotent stem cell derived cardiomyocytes in vitro–correlation between contraction force and electrophysiology. Biomaterials 2015;51:138–50.

[14] Zalk R, Clarke OB, des Georges A, Grassucci RA, Reiken S, Mancia F, et al. Structure of a mammalian ryanodine receptor. Nature 2015;517(7532):44–9.

[15] Peng W, Shen H, Wu J, Guo W, Pan X, Wang R, et al. Structural basis for the gating mechanism of the type 2 ryanodine receptor RyR2. LID - aah5324 [pii]. Science 2016;354(6310).

[16] Yamazaki M, Osaka T, Yokoyama E, Kodama I. A case of short-coupled variant of torsade de pointes characterized by spatial heterogeneity of action potential duration and its restitution kinetics. J. Int. Cardiac Electrophysiology 2006;17(1):35–40.

[17] Dunnink A, Stams TRG, Bossu A, Meijborg VMF, Beekman JDM, Wijers SC, et al. Torsade de pointes arrhythmias arise at the site of maximal heterogeneity of repolarization in the chronic complete atrioventricular block dog. EP Europace 2016;19(5):858–65.

[18] Jung CB, Moretti A, Mederos y Schnitzler M, Iop L, Storch U, Bellin M, et al. Dantrolene rescues arrhythmogenic RYR2 defect in a patient-specific stem cell model of catecholaminergic polymorphic ventricular tachycardia. EMBO Mol Med 2012;4(3):180–91.

[19] BRANDT RR, SHEN W-K. Bradycardia-Induced Polymorphic Ventricular Tachycardia After Atrioventricular Junction Ablation for Sinus Tachycardia-Induced Cardiomyopathy. J Cardiovasc Electrophysiol 1995;6(8):630–3.

[20] Fleming S, Thompson M, Stevens R, Heneghan C, Pluddemann A, Maconochie I, et al. Normal ranges of heart rate and respiratory rate in children from birth to 18 years of age: a systematic review of observational studies. Lancet 2011;377(9770):1011–8.

[21] Grais IM, Sowers JR. Thyroid and the heart. Am J Med 2014;127(8):691–8.

[22] Signore S, Sorrentino A, Ferreira-Martins J, Kannappan R, Shafaie M, Del Ben F, et al. Inositol 1, 4, 5-trisphosphate receptors and human left ventricular myocytes. Circulation 2013;128(12):1286–97.

[23] Swift F, Magnus Aronsen J, Stokke MK, Hougen K, Egger M, Roderick HL, et al. IP3 Receptors in Heart Failure: arrhythmogenic Troublemakers or SR Calcium Security Valves? Biophys. J. 2012;102(3, Supplement 1):101a.

[24] Santulli GA-OX, Nakashima R, Yuan Q, Marks AR. Intracellular calcium release channels: an update. J Physiol 2017;595(10):3041–51.

[25] Nakayama H, Bodi I, Maillet M, DeSantiago J, Domeier TL, Mikoshiba K, et al. The IP3 receptor regulates cardiac hypertrophy in response to select stimuli. Circ Res 2010;107(5):659–66.

[26] Itzhaki I, Rapoport S, Huber I, Mizrahi I, Zwi-Dantsis L, Arbel G, et al. Calcium handling in human induced pluripotent stem cell derived cardiomyocytes. PLoS ONE 2011;6(4):e18037.

[27] Betzenhauser MJ, Fike Jl, Fau - Wagner 2nd LE, Wagner 2nd Le, Fau - Yule DI, Yule DI. Protein kinase A increases type-2 inositol 1,4,5-trisphosphate receptor activity by phosphorylation of serine 937. J Biol Chem 2009;284(37):25116–25.

[28] Devalla HD, Gelinas R, Aburawi EH, Beqqali A, Goyette P, Freund C, et al. TECRL, a new life-threatening inherited arrhythmia gene associated with overlapping clinical features of both LQTS and CPVT. EMBO Mol Med 2016;8(12):1390–408.

[29] Park S-J, Zhang D, Qi Y, Li Y, Lee Keel Y, Bezzerides Vassilios J, et al. Insights Into the Pathogenesis of Catecholaminergic Polymorphic Ventricular Tachycardia From Engineered Human Heart Tissue. Circulation 2019;140(5):390–404.

[30] Di Pasquale E, Lodola F, Miragoli M, Denegri M, Avelino-Cruz JE, Buonocore M, et al. CaMKII inhibition rectifies arrhythmic phenotype in a patient-specific model of catecholaminergic polymorphic ventricular tachycardia. Cell Death Dis 2013;4:e843.

[31] Xiao Z, Guo W, Yuen SM, Wang R, Zhang L, Van Petegem F, et al. The H29D Mutation Does Not Enhance Cytosolic Ca2+ Activation of the Cardiac Ryanodine Receptor. PLoS ONE 2015;10(9):e0139058.

[32] Yuchi Z, Lau K, Van Petegem F. Disease mutations in the ryanodine receptor central region: crystal structures of a phosphorylation hot spot domain. Structure 2012;20(7):1201–11.
[33] Kimura M, Fujisawa T, Aizawa Y, Matsuhashi N, Ito S, Nakajima K, et al. An RyR2 mutation found in a family with a short-coupled variant of torsade de pointes. Int. J. Cardiol. 2017;227:367–9.
[34] Beach LY, Goldschlager N, Moss JD, Scheinman MM. Idiopathic Ventricular Fibrillation in a 29-Year-Old Man. Circulation 2017;136(1):112–4.
[35] Tiso N, Stephan DA, Nava A, Bagattin A, Devaney JM, Stanchi F, et al. Identification of mutations in the cardiac ryanodine receptor gene in families affected with arrhythmogenic right ventricular cardiomyopathy type 2 (ARVD2). Hum. Mol. Genet. 2001;10(3):189–94.
[36] Tiso N, Salamon M, Bagattin A, Danieli GA, Argenton F, Bortolussi M. The binding of the RyR2 calcium channel to its gating protein FKBP12.6 is oppositely affected by ARVD2 and VTSIP mutations. Biochem Biophys Res Commun 2002;299(4):594–8.
[37] Leenhardt A, Glaser E, Burguera M, Nurnberg M, Maison-Blanche P, Coumel P. Short-coupled variant of torsade de pointes. A new electrocardiographic entity in the spectrum of idiopathic ventricular tachyarrhythmias. Circulation 1994;89(1):206–15.
[38] Watanabe H, Chopra N, Laver D, Hwang HS, Davies SS, Roach DE, et al. Flecainide prevents catecholaminergic polymorphic ventricular tachycardia in mice and humans. Nat Med 2009;15(4):380–3.